https://doi.org/10.5194/egusphere-2026-5554
Preprint. Discussion started: 5 November 2026
© Author(s) 2026. CC BY 4.0 License.

Flow dependence of boundary-layer scheme parameters revealed by stochastic inversion

Magdalena Fritz[1], Stefano Serafin[1], Tomislava Vukicevic[2], and Martin Weissmann[1]

[1]Department of Meteorology and Geophysics, University of Vienna, Vienna, Austria
[2]Faculty of Physics, University of Belgrade, Belgrade, Serbia

Correspondence: Magdalena Fritz (m.fritz@univie.ac.at)

Abstract. Planetary boundary layer (PBL) parameterization schemes rely on empirical parameters that are typically assumed to be spatially and temporally invariant. In this study, instead of seeking a single optimal parameter as in conventional calibration, we investigate whether optimal PBL parameters exhibit flow dependence under controlled conditions. We consider the simplest prototype of flow dependency in the atmospheric PBL, specifically surface heating impacting the near-surface potential temperature profile. We apply a generalized stochastic inverse modeling technique to characterize the flow-dependent behavior of parameters governing vertical mixing and entrainment in a first-order turbulence closure, the YSU boundary layer scheme. Using the Weather Research and Forecasting (WRF) model in single-column configuration, we characterize model uncertainty from ensembles of perturbed simulations and observational uncertainty from LES output, treated here as the virtual truth providing synthetic observations. These two sources of uncertainty, together with prior knowledge on the parameters, are combined within the inverse estimation framework to obtain posterior distributions of PBL parameters. The results demonstrate that optimal PBL parameters vary with the atmospheric state. Multi-parameter experiments further reveal that different (independent) parameters can have correlated impacts on the modelled state of the PBL. The inferred joint posterior distributions provide a physically informed basis for representing parameter uncertainty in stochastic and perturbed-parameter schemes. Such dependencies are not captured by traditional perturbed-parameter ensembles that independently sample each parameter from a predetermined prior distribution. Beyond its application to uncertainty representation, we show that the stochastic inversion approach provides the theoretically optimal reference for evaluating ensemble-based parameter estimation methods. These methods become necessary for high-dimensional parameter spaces where the stochastic inversion becomes computationally intractable.

1 Introduction

Planetary boundary layer (PBL) parameterization schemes are indispensable components of numerical weather prediction (NWP) and climate models (Ayotte et al., 1996). They represent subgrid-scale turbulent processes using closure assumptions (Stull, 1988; Stensrud, 2007) that are often based on empirical data (e.g., field campaigns, laboratory experiments, or idealized high-resolution simulations) and depend on uncertain parameters. Model errors caused by PBL parameterizations are partly

https://doi.org/10.5194/egusphere-2026-5554
Preprint. Discussion started: 5 November 2026
© Author(s) 2026. CC BY 4.0 License.

structural (due to oversimplified closure assumptions) and partly parametric (due to sub-optimal specification of parameter values).

The simplest approach to parameterize turbulent exchange in the PBL is local first-order closure, in which turbulent fluxes at each model grid point are assumed to be proportional to the spatial gradients of resolved-scale atmospheric variables at that point, through an eddy diffusivity coefficient K. However, strong convective conditions require nonlocal formulations to properly represent vertical mixing by large turbulent eddies. An early example of nonlocal closure is the model by Troen and Mahrt (1986), who prescribed a power-law eddy diffusivity profile (O'Brien, 1970) and used a countergradient flux term to represent the transport by rising plumes (Ertel, 1942). In later implementations and further refinements of the parameterization scheme (Noh et al., 2003; Hong et al., 2006), the empirical parameters were derived from large-eddy simulations (LES).

The common assumption that optimal parameter values are spatially and temporally invariant, i.e., global parameters, is a cause of parameteric error. Even if the functional form of the parameterization is assumed to be correct, optimal parameter values are not inherently universal - they are merely chosen as such, but they may equally well depend on the flow conditions. The values of optimal parameters can be inferred from observations by solving an inverse problem (Tarantola and Valette, 1982; Mosegaard and Tarantola, 2002; Tarantola, 2005). In deterministic approaches, an inverse problem is often formulated as an optimization problem that minimizes the discrepancy between model-predicted outputs and observations (Tarantola, 2005). Many inverse problems of this form are ill-posed, as the observations may not uniquely determine the parameters. To render the problem well-posed, regularization methods (Tikhonov et al., 1995) are typically applied to address the nonuniqueness. Another way of addressing nonuniqueness was introduced by Backus and Gilbert (1970). Instead of selecting one of many possible solutions through a priori constraints, as in regularization, they devised a method for calculating unique localized averages of the solution. Both the reduction to a single point estimate inherent to regularization and the neglect of prior information in the Backus–Gilbert method motivated the general stochastic formulation of the inverse problem by Tarantola and Valette (1982), which was later extended by Mosegaard and Tarantola (2002). Therein, the inverse problem is recast as a combination of different and independent states of information on the model parameters, drawn from both observations and prior knowledge. The result is a posterior distribution of the model parameters, from which statistical measures can be computed to characterize parameter uncertainties. Similar to standard Bayesian statistical estimation theory (Bolstad and Curran, 2007; Bennett, 1992; Evensen, 2006; van Leeuwen and Evensen, 1996), the formulation of Mosegaard and Tarantola (2002) assigns a probability density function (PDF) to each quantity that contributes to the overall knowledge of the modeled and observed states of the system. Distinctively, it represents the model and its errors (e.g., via an ensemble), the observation errors, and the prior information as separate PDFs, allowing each component's contribution to be uniquely identified. The Bayesian approach is the special case of the general framework obtained by treating the forward relation as exact - rather than as a genuinely uncertain theoretical prediction - and the homogeneous probability density as constant (i.e., null information represented by a uniform distribution). Mosegaard (2011) showed that these simplifications involve a conditioning operation that can yield inconsistent results.

While the Bayesian approach has been more widely adopted in atmospheric sciences (Grund and Schemm, 2026), including climate modeling (Dunbar et al., 2021; Howland et al., 2022), turbulence parameterization (Shin and Howland, 2026; Edeling

https://doi.org/10.5194/egusphere-2026-5554
Preprint. Discussion started: 5 November 2026
© Author(s) 2026. CC BY 4.0 License.

et al., 2014), and cloud microphysics parameterization (Kim et al., 2026), the general inverse theory has its origin in seismology (Tarantola, 1984; Charara et al., 2000; Crase et al., 1992). Vukicevic and Posselt (2008) demonstrated the applicability of this formulation to simplified atmospheric physics models. Subsequent studies applied the method to assess uncertainty in cloud microphysical parameters (Posselt and Vukicevic, 2010) and to estimate parameter uncertainty in a hurricane model (Rios-Berrios et al., 2014). These studies also examined relationships between parameters through their joint distributions, which can be informative for the development of stochastic parameterizations (Berner et al., 2017; Vukicevic et al., 2022).

In this study, we use the generalized stochastic inversion approach to demonstrate that the optimal values of global parameters in a first-order turbulence closure, the YSU scheme (Hong et al., 2006), vary even when all system properties are stationary and homogeneous except the lower boundary conditions. We consider the YSU scheme because it only depends on global parameters, and it provides a simple yet reasonably realistic method for parameterizing turbulence. This approach provides the most generalized estimate of optimal parameters, as it does not rely on assumptions about the functional form of the parameter dependence. This makes it useful for informing stochastic parameterizations and providing a reference point against which other estimation methods can be compared. To our knowledge, this is the first application of the general stochastic inversion approach to PBL parameterization.

Our idealized modelling environment uses the Weather Research and Forecasting (WRF) model version 4.4.2 (Skamarock et al., 2019). Model and observation PDFs are generated using the single-column model (SCM) and large-eddy simulation (LES) configurations, respectively, with ensemble SCM runs used to characterize model errors.

The remainder of this paper is organized as follows: the target parameterization and its parameters of interest are introduced in Sect. 2.1. Section 2.2 briefly introduces the inverse estimation approach, but we refer the reader to Vukicevic and Posselt (2008) for a detailed description of the algorithm. We present the simulations used to generate the necessary PDFs for the experiments in Sect. 2.3. A simple sensitivity analysis (Sect. 3) precedes the application of the general stochastic inverse estimation approach in Sect. 4. In Sect. 5, we discuss the results in detail, examining their relevance for stochastic parameterizations and drawing comparisons to other inversion methods.

2 Theoretical framework

2.1 PBL parameterization

The YSU scheme (Hong et al., 2006) is a non-local first-order turbulence parameterization. It accounts for three contributions to vertical mixing: a local mixing term proportional to the local gradient and two nonlocal terms representing countergradient transport and entrainment fluxes at the top of the PBL, respectively. The YSU scheme differs from other first-order closures because of the explicit treatment of the entrainment process. It is computationally efficient, because it does not use any prognostic equation for second- or higher-order turbulence moments, and it is one of the most tested and validated PBL schemes in WRF (Hu et al., 2013). It is known to be comparatively inaccurate in stable boundary layer conditions (Storm et al., 2009).

https://doi.org/10.5194/egusphere-2026-5554
Preprint. Discussion started: 5 November 2026
© Author(s) 2026. CC BY 4.0 License.

In the YSU scheme, Hong et al. (2006) define the turbulent diffusion of a prognostic variable C as:

$$\frac{\partial C}{\partial t} = \frac{\partial}{\partial z}\left[K_c\left(\frac{\partial C}{\partial z} - \gamma_c\right) - \overline{w'c'_h}\left(\frac{z}{h}\right)^3\right], \tag{1}$$

where K_c is the eddy diffusion coefficient, γ_c is a correction to the local gradient, and z and h represent the height above ground and the boundary-layer depth, respectively. The rightmost term of Eq. 1 is an explicit representation of the entrainment flux. As in Troen and Mahrt (1986), the following closure assumption for the eddy coefficient is used:

$$K_C = \kappa w_s z\left(1 - \frac{z}{h}\right)^p, \tag{2}$$

where κ is the von Kármán constant, w_s is the mixed-layer velocity scale and p is an empirical parameter. The countergradient term is given by:

$$\gamma_c = b\frac{\overline{w'c'}_0}{w_{s0}h}, \tag{3}$$

where $\overline{w'c'}_0$ is the surface flux of quantity C, w_{s0} is the mixed-layer velocity scale at z = 0.5 h, and b is an empirical proportionality coefficient. The entrainment flux is expressed by

$$\overline{w'c'_h} = -A_e\frac{\theta_{va}}{g}\frac{w_m^3}{h}, \tag{4}$$

where θ_{va} is the virtual potential temperature at the lowest model level, g is the gravitational acceleration, w_m is a velocity scale based on the surface layer turbulence, and A_e is another empirical parameter. The three velocity scales w_s, w_{s0} and w_m are parameterized quantities (see Hong et al., 2006). They depend on the atmospheric flow, on surface properties, and on surface fluxes, but they are independent of the empirical parameters p, b, and A_e.

The prescribed values of the parameters, p (= 2.0), b (= 6.8), and A_e (= 0.15), are taken partly from preceding literature on first-order closure schemes (Troen and Mahrt, 1986; Brost and Wyngaard, 1978; Holtslag and Boville, 1993; Pleim, 2007; de Roode et al., 2004), and partly from a subjective evaluation of the agreement between parameterization output and LES data (Noh et al., 2003).

2.2 Inverse estimation approach

This study employs the general stochastic inverse theory as introduced by Mosegaard and Tarantola (2002). The theory rests on combining three types of information, all expressed as probability distributions in a joint space of model parameters **m** and observed data $\mathbf{y}^o$. Throughout this study, f denotes a PDF. The three types of information are: (1) prior information on the model $f(\mathbf{m})$, carrying information we have on **m**, (2) physical theory linking model to data (via a forward model), expressed as a joint probability $f(\mathbf{y}^b, \mathbf{m})$, where $\mathbf{y}^b$ denotes the model-predicted data (model equivalents), and (3) uncertain observations described by $f(\mathbf{y}^o)$. Multiplication of the model-based PDF $f(\mathbf{y}^b, \mathbf{m})$, in a joint space of observation and parameter values, with the observation-based PDF $f(\mathbf{y}^o)$ yields a joint posterior PDF $f(\mathbf{y}^b, \mathbf{m}, \mathbf{y}^o)$. The optimal parameter estimate is, by definition, the location in $f(\mathbf{y}^b, \mathbf{m}, \mathbf{y}^o)$ with the greatest probability density. The error characteristics for each parameter in vector **m**

https://doi.org/10.5194/egusphere-2026-5554
Preprint. Discussion started: 5 November 2026
© Author(s) 2026. CC BY 4.0 License.

can be analyzed by considering its marginal posterior probability distribution $f_m(\mathbf{m})$. $f_m(\mathbf{m})$ is computed by integrating the joint posterior PDF $f(\mathbf{y}^b, \mathbf{m}, \mathbf{y}^o)$ over the observation space. By conditioning the functional relationship on two parameters simultaneously, $f(\mathbf{y}^b, \mathrm{m}_1, \mathrm{m}_2)$, the joint posterior $f(\mathbf{y}^b, \mathrm{m}_1, \mathrm{m}_2, \mathbf{y}^o)$ can be computed. This captures the correlation between the impacts of different parameters on the model state - hereafter referred to as parameter correlations (see Sect. 4.2).

The numerical algorithm we employ in this study to calculate posterior PDFs of parameters is described in detail in Vukicevic and Posselt (2008). We provide a short summary of the important equations in the Appendix A. Here, we adopt the method to estimate turbulence parameters in the YSU scheme. Ingesting observations from multiple time steps yields a marginal posterior PDF at each time step, allowing the evolution of the optimal parameter estimates (and their error characteristics) to be tracked over time.

2.3 Experimental design

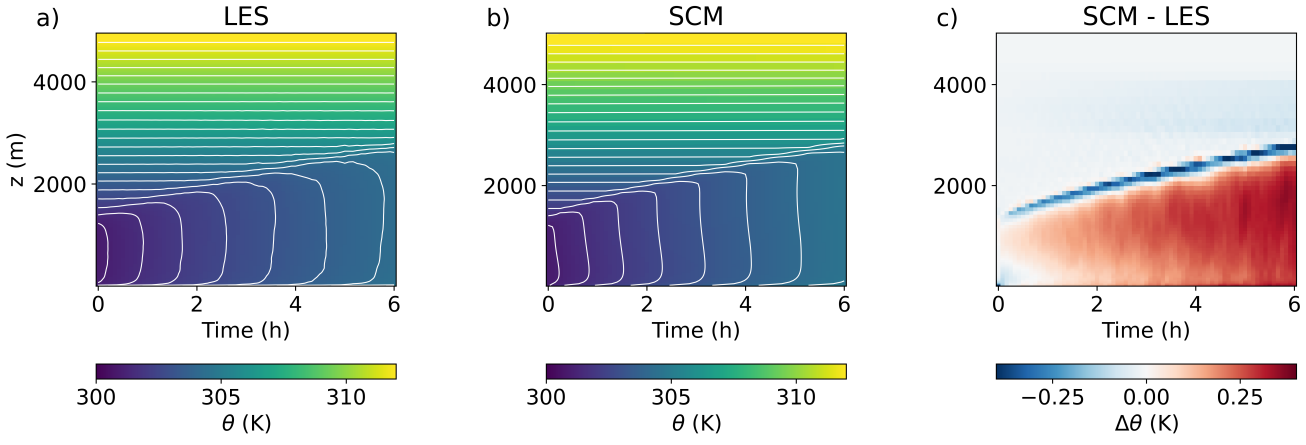


Figure 1. Temporal evolution of θ over 6 hours for a convective PBL. Panel a) shows the domain-averaged θ from the LES simulation. Panel b) shows the SCM run with prescribed YSU parameters. Panel c) shows the difference (SCM - LES), with the LES field interpolated onto the (coarser) SCM vertical grid prior to differencing. White lines in a) and b) represent θ contours every 0.5 K.

2.3.1 Observations

In this study, synthetic observations are drawn from an LES generated with the WRFlux software package (Göbel et al., 2022). The LES serves as the virtual truth in the experiments and is referred to as the nature run. Figure 1a shows the temporal evolution of θ over 6 hours for a convective PBL forced by a constant, uniform surface sensible heat flux ($\overline{w'\theta'}_0$ = 0.24 Km s^{-1}) and a constant geostrophic wind (U_g = 5 m s^{-1}), mimicking one of the reference simulations originally used to tune the parameters of the YSU scheme (Noh et al., 2003). The model domain is 5 km x 5 km with a horizontal resolution of Δx = 20 m. In the vertical, the computation domain extends over 5000 m, with grid spacing $\Delta z \approx$ 20 m. Lateral boundary conditions

https://doi.org/10.5194/egusphere-2026-5554
Preprint. Discussion started: 5 November 2026
© Author(s) 2026. CC BY 4.0 License.

are periodic in the x direction, and a Rayleigh damping layer is applied at the domain top to suppress spurious gravity wave reflection. The initial temperature stratification is neutral up to $z = 850$ m and stable (3.0 K km^{-1}) aloft.

In the following analysis, we consider potential temperature observations, since they are sensitive to changes in turbulence parameter values (see Sect. 3). They consist of vertical profiles, spatially averaged over the LES domain and sampled at 43 equally spaced levels between $z = 100$ m and $z = 3000$ m. The observation uncertainty is obtained by fitting a Gaussian distribution to the LES θ values sampled across all horizontal grid points, characterized by their sample mean and standard deviation.

2.3.2 Ensemble

Solving an inverse problem generally requires sufficient sampling of the parameter space N^M, where N is the resolution of the parameter space (here N = 30 bins) and M is the number of control parameters (Posselt and Vukicevic, 2010), here M = 3. Because the parameters are global, they have uniform values at all model grid points. Following Rios-Berrios et al. (2014), who sampled a two-dimensional parameter space with 30^2 simulations, we adopt the same sample size per dimension and use 30^3 (= 27 000) simulations for our three control parameters. As our focus is on characterizing flow-dependent structure in parameter sensitivity rather than on obtaining precise point estimates, this ensemble size is sufficient to resolve the relevant trends. The use of the WRF SCM allows for such a large ensemble. The ensemble is subject to simultaneous perturbations of parameters p, b, and A_e, each drawn from uniform distributions (Table 1). The ranges of these distributions were informed by educated guesses and sensitivity analyses as explained in Sect. 3. Parameter values are drawn using Sobol sequences (Saltelli et al., 2010), which guarantee a more uniform coverage (and no repetitions) of the parameter space compared to random sampling. In all ensemble simulations, the initial atmospheric condition and the boundary condition (i.e., the surface forcing imposed on the SCM integrations) are the same for all members and coincide with the LES configuration described in Sect. 2.3.1.

3 Sensitivity of the PBL state to parameters

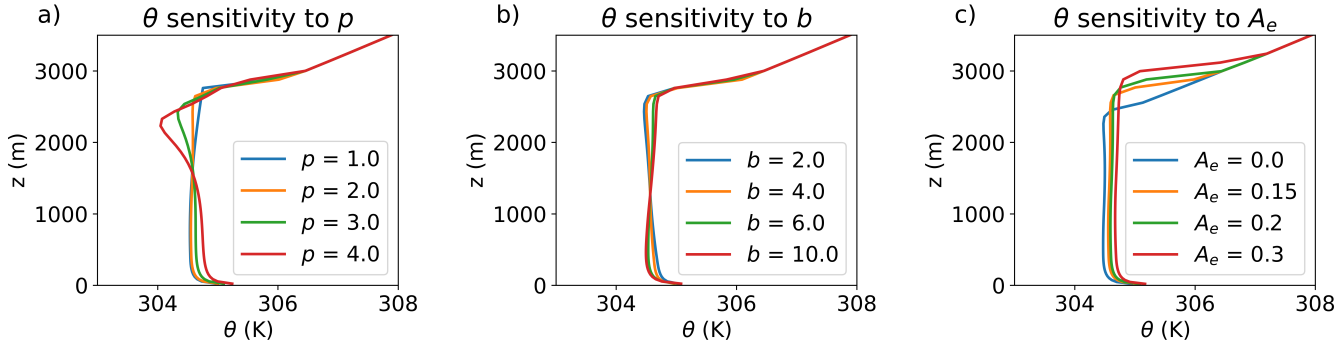


Figure 2. Impact of a parameter on the modelled state. θ profiles for different values of a) p, b) b, and c) A_e after a six-hour model integration.

https://doi.org/10.5194/egusphere-2026-5554
Preprint. Discussion started: 5 November 2026
© Author(s) 2026. CC BY 4.0 License.

We focus on parameters p, b, and A_e because they determine the parameterized vertical turbulent mixing in the bulk of the PBL. Because the inverse estimation approach (Mosegaard and Tarantola, 2002) is a computationally demanding exercise associated with sufficient sampling of the joint parameter-state space, it is useful to first explore the sensitivity of the modelled PBL state to the values of the three empirical parameters in a simpler way, i.e., by perturbing the individual parameters independently.

Figure 2 is based on 6-hour SCM simulations, assuming a constant sensible heat flux of 0.24 Km s^{-1} and a constant mean wind speed of 5.0 m s^{-1}, and it illustrates the sensitivity of potential temperature profiles to different parameter values. Low p values create a deep PBL with slightly stable stratification, whereas high p values tend to generate a statically unstable PBL (Fig. 2a). Figure 2b shows that parameter b has little effect on the PBL depth compared to p, but mainly influences stability. In contrast to parameter p, lower values of b result in a statically unstable PBL, whereas higher b yield a stably stratified PBL. For the entrainment flux parameter A_e, the region of highest sensitivity is found at the top of the PBL (Fig. 2c). High A_e values imply stronger downward heat flux from the free atmosphere, and thus tend to create a deeper and warmer PBL. Stability in the core of the convective PBL is not affected appreciably by A_e. Figures 2a-c inform the selection of plausible ranges for the prior parameter distributions (Table 1). We assume the prior state of all parameters to be described by a bounded uniform distribution. This is nearly noninformative, i.e., it does not assume any preferential parameter value in the admitted range.

Table 1. YSU scheme parameters and their prior distributions.

Parameter	YSU value	Plausible range	Role of parameter
p	2.0	$U(0.5, 4.0)$	Controls eddy diffusivity profile
b	6.8	$U(0.0, 10.0)$	Controls magnitude of countergradient correction
A_e	0.15	$U(0.0, 0.3)$	Controls entrainment rate

4 Results

4.1 Probabilistic assessment of flow-dependent turbulence parameters

The numerical algorithm for computing the posterior PDF of parameter estimates following Vukicevic and Posselt (2008) is illustrated in Fig. 3. We demonstrate the method using a single observation at a specific time (t = 6 h) and height ($z \approx 1000$ m) to constrain parameter p. Figure 3a shows the assumed Gaussian PDF for a single θ observation, as introduced in Sect. 2.3. The measurement and parameter spaces are discretized using N = 30 evenly spaced bins. Fig. 3b depicts the joint model PDF of the model equivalents $\mathbf{y}^b$ and the control parameter p. Multiplying this PDF with the measurement PDF combined with the prior information on the parameter $f(p)$, which is assumed to be uniform, yields the joint posterior PDF in Fig. 3c. The multiplication reinforces regions of overlapping high density around the mean potential temperature ($\sim$ 304.2 K) while reducing the prior

https://doi.org/10.5194/egusphere-2026-5554
Preprint. Discussion started: 5 November 2026
© Author(s) 2026. CC BY 4.0 License.

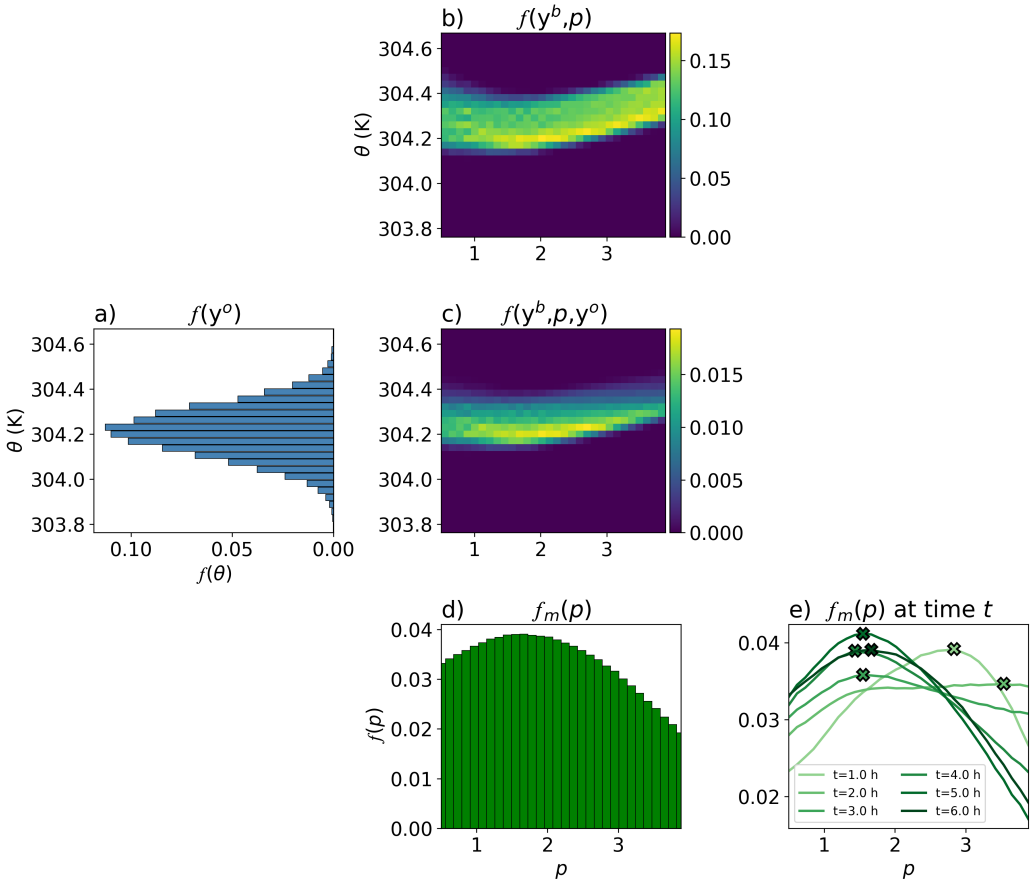


Figure 3. Inverse estimation of parameter p from a single observation. a) PDF of the θ observation $f(y^o)$ (see Sect. 2.3.1). b) Joint model PDF $f(y^b,p)$. c) Joint posterior PDF $f(y^b,p,y^o)$. d) Normalized marginal posterior PDF for parameter p, $f_m(p)$. e) Evolution of $f_m(p)$ over time.

density elsewhere. Subsequent marginalization over θ and normalization yields the posterior marginal PDF in parameter space $f_m(p)$ in Fig. 3d. Since the prior is uniform, it contributes only a normalization factor and therefore does not affect the shape of the posterior. Fig. 3e extends the analysis in time, showing the normalized marginal PDFs of the same parameter after ingesting θ observations at the same height over a time interval. We find that both the optimal parameter estimate (marked by green crosses) and the shape of the distributions evolve over time. While higher values of p appear to better represent the state of the PBL in the first two hours, the optimal estimate shifts below $p = 2$ as time progresses.

https://doi.org/10.5194/egusphere-2026-5554
Preprint. Discussion started: 5 November 2026
© Author(s) 2026. CC BY 4.0 License.

Figure 4 extends the analysis of Fig. 3e by aggregating the marginal PDFs over all heights (see Sect. 2.3) up to time t (Δt = 5 min), with the posterior PDF from each observation normalized to integrate to 1 before aggregation. Marginal posterior distributions are shown for parameters p (Fig. 4a), b (Fig. 4b), and A_e (Fig. 4c). As more observations are ingested over time, the posterior distributions become narrower (highest posterior probability in darker regions), indicating increasingly strong constraints on the parameters. All three panels start from a uniform distribution at t = 0 h, with each bin assigned equal probability $1/N = 1/30$.

Parameter p (Fig. 4a) exhibits a clear shift toward lower optimal values ($p \sim 1.8$) over the 6 hours and increasing concentration of posterior probability. In contrast, optimal estimates for parameter b (Fig. 4b) increase from $b \sim 2.5$ to $b \sim 6$ with a broader posterior distribution throughout the observation period, suggesting greater uncertainty and weaker constraints by the available observations. Parameter A_e (Fig. 4c) remains confined to a narrow range, with its posterior concentrated just below A_e = 0.1 from early times onward. Its consistently narrow distribution indicates that it is the best-constrained of the three parameters. Despite the large number of observations informing each marginal, the posterior probability ranges in Fig. 4 remain comparatively broad. This can be explained by the shape of the joint PDF in Fig. 3b, which shows that the state (ordinate axis) is only weakly sensitive to changes in the parameters (abscissa). Together with the relatively uncertain observations (Fig. 3a), this limits how much information each additional observation contributes.

To assess whether the identified parameter trends are robust to a reduced observation frequency, as would be the case in an operational ensemble filter, where assimilation cycles are typically on the order of hours rather than minutes, Figs. 4d-f show the instantaneous marginal distributions at time t averaged over hourly intervals. Despite ingesting observations at a coarser temporal resolution, the overall trends identified in Figs. 4a-c are consistent: p shifts to lower values and b increases. Hourly averages reveal a decreasing trend in A_e over the first 3 hours, followed by a sustained, gradual increase. The overall shape of the distributions is similarly preserved, suggesting little loss of information at coarser temporal resolution. Consequently, both the optimal parameter estimates and their associated uncertainty characteristics should remain trackable under operationally realistic update intervals.

4.2 Joint posterior distributions of parameter pairs

As mentioned in Sect. 2.2, we can compute pairwise joint posterior distributions $f(\mathrm{m}_1,\mathrm{m}_2,\mathbf{y}^o)$ to capture parameter correlations. In Figure 5, we show posterior joint PDFs, aggregated over height and time for each possible parameter pair, using the same ensemble as in Sect. 4.1. The joint posterior distributions obtained with stochastic inversion are not constrained to any specific functional form. In fact, they can be particularly complex. Examples of multimodality, implying non-uniqueness of optimal parameter values, have been reported in the literature (e.g., Posselt and Vukicevic, 2010). However, the joint posterior distributions for the three parameters of the YSU scheme (Fig. 5) can be approximated reasonably well with two-dimensional Gaussian distributions. Many filters commonly used in atmospheric data assimilation (e.g., ensemble filters Evensen, 2006) rely on Gaussianity assumptions, and fitting a two-dimensional Gaussian to the joint PDFs allows us to approximate how such filters would perceive the correlation structure between parameters. The parameters of the fitted Gaussian are then used to derive the correlation coefficient r for each parameter pair.

https://doi.org/10.5194/egusphere-2026-5554
Preprint. Discussion started: 5 November 2026
© Author(s) 2026. CC BY 4.0 License.

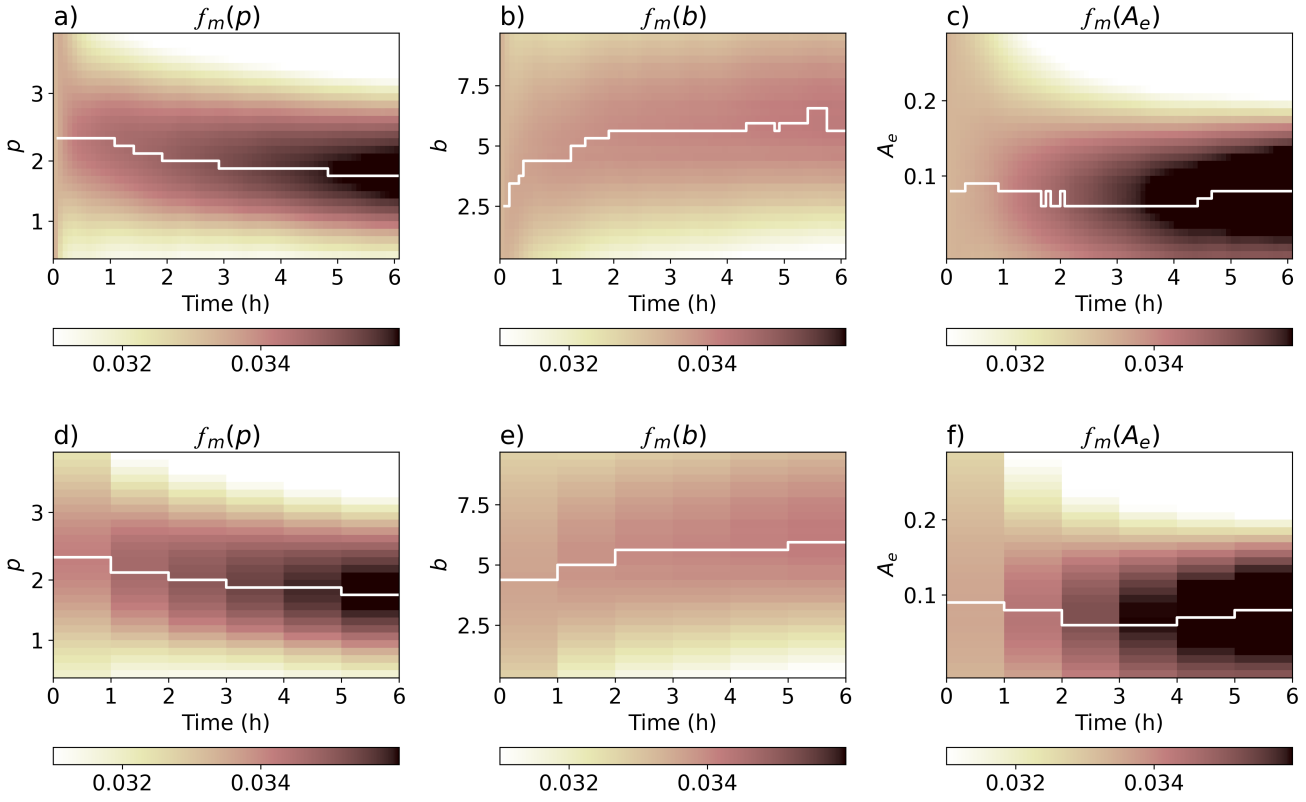


Figure 4. Aggregated posterior marginal distributions $f_m(\mathbf{m})$ over height. Panels a-c show marginal distributions for parameter a) p, b) b, and c) A_e up to time t. Panels d-f show hourly averaged marginal distributions for parameter d) p, e) b, and f) A_e. The white lines in each panel highlight the maximum posterior estimate.

For $f(p,b,\mathbf{y}^o)$ in Fig. 5a, the area of highest posterior density is elongated along the lower-left to upper-right diagonal, indicating a positive parameter correlation between the optimal values of p and b. This is quantified by the positive correlation coefficient derived from the two-dimensional Gaussian fit, which yields r = 0.51. The relationship implies that observations cannot uniquely identify p and b independently; instead, the data constrain a coupled relationship, suggesting a shared underlying mechanism. Within this diagonal region, the darkest pixels, corresponding to the highest posterior density, cluster around p $\sim$ 1.0 - 2.5, which is consistent with the maximum posterior estimates in Fig. 4. For b, the posterior is less tightly constrained, which also reflects the results in Fig. 4.

As for $f(p,A_e,\mathbf{y}^o)$ in Fig. 5b, the area of highest posterior density is concentrated around $p \sim$ 0.5 - 2.5 and $A_e \sim$ 0.0 - 0.15, with decreasing density toward the upper ranges of both parameters. The upward-sloping contour lines indicate a positive relationship between optimal values of p and A_e. This is confirmed by the correlation coefficient derived from the fitted Gaussian, r = 0.36, which points to a moderate positive correlation.

https://doi.org/10.5194/egusphere-2026-5554
Preprint. Discussion started: 5 November 2026
© Author(s) 2026. CC BY 4.0 License.

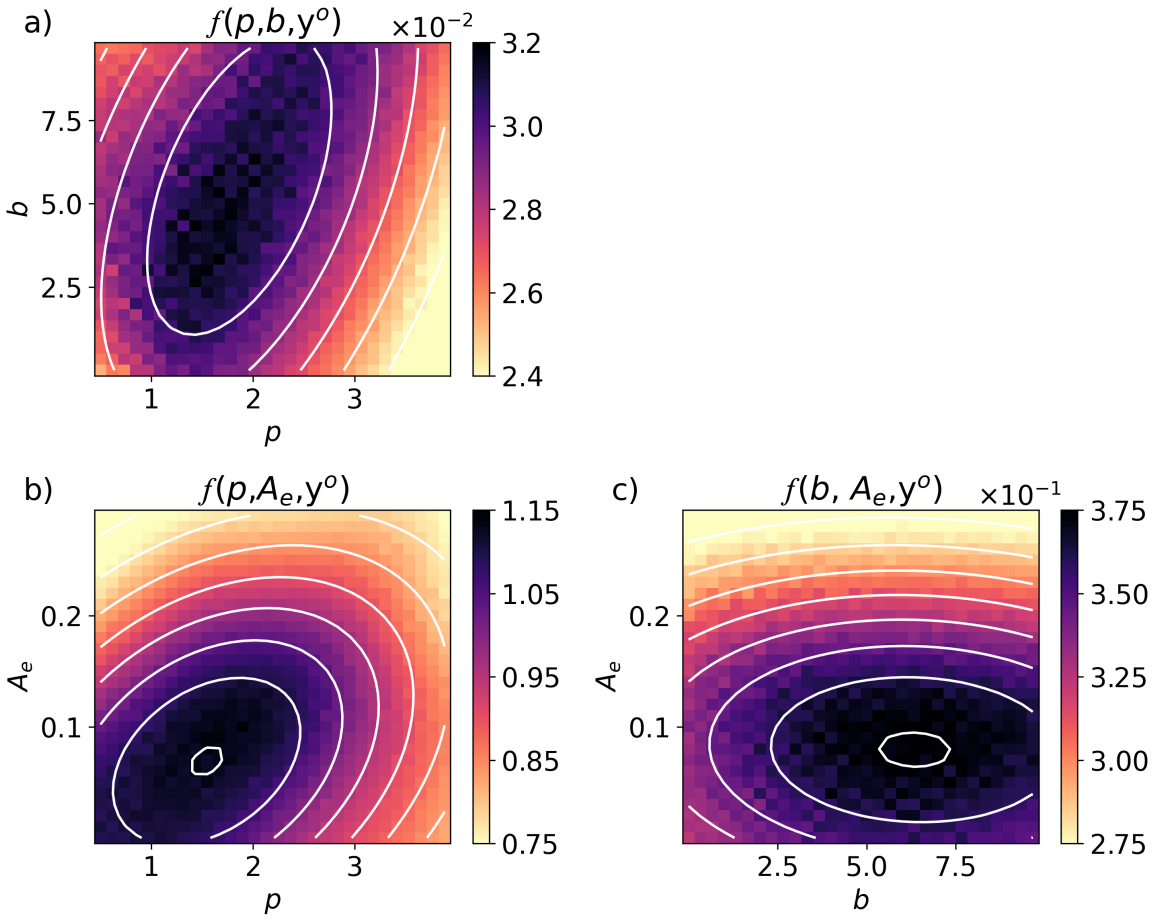


Figure 5. Aggregated joint posterior distributions $f(\mathrm{m}_1,\mathrm{m}_2,\mathbf{y}^o)$ for the three parameter pairs a) p-b, b) p-A_e, and c) b-A_e over height and time. White contour lines mark isodensity levels at intervals of ~ 0.1 times the maximum value, based on a two-dimensional Gaussian fitted independently to each joint posterior. Note that the colorbar differs across panels.

The joint posterior distribution $f(b,A_e,\mathbf{y}^o)$ in Fig. 5c shows little evidence of a correlation between b and A_e: the Gaussian fit correlation coefficient yields r = - 0.05. The high-density region is roughly a horizontal band concentrated around $A_e \sim 0.1$ (cf. Fig. 4), and extends across a wide range of b. This indicates that here, too, A_e is better constrained by the observations than b (cf. Fig. 4). Despite both of the parameters being individually related to p (Figs. 5a and 5b), the posterior distribution of A_e and b inferred from θ observations shows no evidence of correlation between them.

The broad regions of high density around the optimal estimates across the three panels imply that different combinations of parameter values explain the data equally well, such that finding unique optimal values is difficult. The relative peak densities

https://doi.org/10.5194/egusphere-2026-5554
Preprint. Discussion started: 5 November 2026
© Author(s) 2026. CC BY 4.0 License.

- highest for $f(p,A_e,\mathbf{y}^o)$, intermediate for $f(b,A_e,\mathbf{y}^o)$, and lowest for $f(p,b,\mathbf{y}^o)$ - reflect the fact that each joint posterior is normalized by its bin widths, so parameters with smaller bin areas (i.e., A_e) yield correspondingly higher peak densities.

5 Discussion

Based on the results presented so far, we first discuss the dependence of optimal parameters on the flow, leaving a detailed physical interpretation of optimal values to future work. We then examine the implications of the identified parameter relationships for stochastic parameterizations. Finally, we compare the stochastic inversion approach to alternative methods.

5.1 Flow-dependent parameters

The results presented in Sect. 3 and 4.1 reveal that parameters governing vertical mixing in the YSU scheme are flow-dependent rather than universal. As demonstrated in the simple sensitivity analysis using single SCM runs in Fig. 2, varying the target parameters in the YSU scheme affects the stratification (mainly p and b) and the depth (mainly A_e) of the PBL. The most likely parameter values we seek by solving the inverse problem in Sect. 4.1 coincide with the ranges that produce a well-mixed PBL (Fig. 2), with a capping inversion just as strong as in the nature run (Fig. 1a).

In Figure 1, we compare the domain-averaged θ evolution from the LES (Fig. 1a) and the SCM run with default parameters (Fig. 1b), and show their difference (Fig. 1c). We compute the difference as SCM minus LES so that positive values indicate a warm bias in the SCM and negative values a cold bias. The difference is predominantly positive throughout the bulk of the PBL ($\sim$ + 0.2 K) and negative near the top of the PBL ($\sim$ - 0.3 K), indicating that the SCM with default parameters is too warm within the mixed layer and underestimates the strength of the capping inversion. This systematic bias motivates the parameter adjustments in Fig. 4, which aim to compensate for these deficiencies.

This suggests that empirical parameters should not be interpreted as universal constants, but rather as a compact way of representing an insufficient level of knowledge of the modelled physical system. Since parameters represent imperfect knowledge, there is no reason to expect them to be unique or invariant. If they are instead locally and dynamically adjusted to the flow, model parameters become additional degrees of freedom that can compensate for structural model errors, making it possible to mimic the behaviour of the actual physical system more accurately.

5.2 Informing perturbed parameter ensembles with parameter correlations

One way to represent uncertainty in climate and weather models is through perturbed-parameter ensembles (PPE: Murphy et al., 2004), which perturb closure parameters in physical process parameterizations to represent uncertainty a priori (Berner et al., 2017). This contrasts with stochastic perturbation schemes, such as the stochastically perturbed parameterization tendency (SPPT) scheme (Weisheimer et al., 2014) or the stochastic kinetic-energy backscatter scheme (SKEBS: Shutts, 2005), which add uncertainty a posteriori to models that have been independently developed and tuned. Traditional PPEs typically perturb each parameter independently (Murphy et al., 2004; Hacker et al., 2011; Reynolds et al., 2011), without accounting for cross-

https://doi.org/10.5194/egusphere-2026-5554
Preprint. Discussion started: 5 November 2026
© Author(s) 2026. CC BY 4.0 License.

covariances between parameters. Perturbed parameters can either be held fixed within an integration but varied across ensemble members (Murphy et al., 2004; Hacker et al., 2011), or allowed to vary in time (Ollinaho et al., 2013).

The results in Sect. 4.2 indicate that the three turbulence parameters are not independent, but that there is a level of correlation between their optimal values. The relationships identified for p-b and p-A_e act as constraints on the system, reducing its effective degrees of freedom. This has direct implications for how parameter uncertainty should be represented in perturbed-parameter schemes. Drawing each parameter independently from its own marginal distribution implicitly assumes that any combination of parameter values is equally plausible. However, the parameter correlations shown in Fig. 5 show that this is not the case.

The positive relationship between p and b emerging from the multiple parameter perturbation experiments (Fig. 5) is consistent with the sensitivities shown in Fig. 2: because p and b have opposing effects on PBL stability, their optimal values are required to co-vary to compensate for one another. For example, in a neutrally stratified mixed layer (Fig. 1b), increasing p destabilizes the profile (K_C increases - Eq. 2); to maintain agreement with the observations, b must increase (stabilize, γ_C increases - Eq. 3) in turn. The positive relationship between p and A_e follows a similar compensatory logic. However, A_e does not meaningfully affect stability but instead governs PBL height (Sect. 3). Consequently, if increasing p slightly suppresses PBL growth (Fig. 2a), then A_e must increase and enhance entrainment to maintain a good match with the observed PBL height (Fig. 1).

The parameter correlations captured by the joint posterior distributions can be used to replace independent-perturbation assumptions in traditional PPE design. Instead of being drawn from independent prior distributions, the parameter values in the ensemble members can be drawn from joint posteriors informed by the observations.

5.3 The stochastic inversion approach as reference methodology

We have shown that meaningful marginal and joint posterior parameter distributions can be obtained using an ensemble of $\mathcal{O}(10^5)$ members that samples a three-dimensional parameter space. Similarly, Rios-Berrios et al. (2014) used an ensemble of $\mathcal{O}(10^3)$ to sample a two-dimensional parameter space. This brute-force approach, however, is only feasible for low-dimensional parameter spaces, i.e., when the forward model depends on a limited number of global parameters. Monte Carlo sampling methods, such as Markov Chain Monte Carlo (MCMC), are generally more computationally efficient and enable inference for more complex parameterizations that depend on a larger number of parameters (Posselt and Vukicevic, 2010). However, even MCMC methods become intractable when the forward model itself is computationally expensive. One option is to replace the forward model with a cheap surrogate, or emulator, trained to reproduce its behaviour (Cleary et al., 2021; Shin and Howland, 2026). Another option is to make the inversion itself cheaper: ensemble-based methods use covariance localization to break the global inversion problem into many local ones (Hacker and Snyder, 2005; Zupanski and Zupanski, 2006), employing ensemble filters (Evensen, 2006) such as the stochastic Ensemble Kalman Filter (EnKF: Evensen, 2006) or the Ensemble Adjustment Kalman Filter (EAKF: Anderson, 2001). The latter approach may be particularly efficient if the parameters are allowed to vary spatially, taking on different values at every grid point, since the dimensionality of the parameter space grows accordingly.

https://doi.org/10.5194/egusphere-2026-5554
Preprint. Discussion started: 5 November 2026
© Author(s) 2026. CC BY 4.0 License.

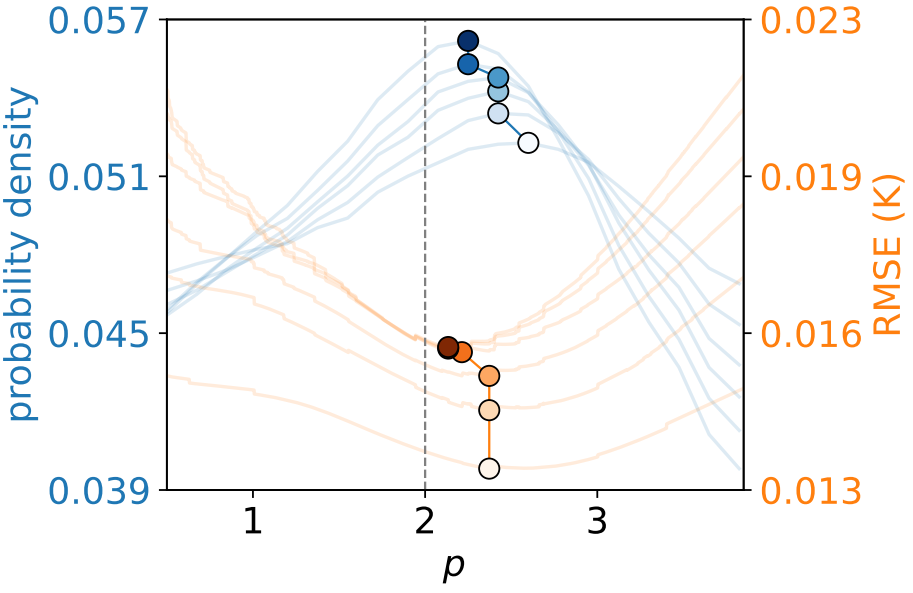


Figure 6. Tracking optimal parameter values using two different estimation methods. Left (blue axis): normalized marginal posterior PDF for parameter p, derived from general inverse theory (light blue curves), aggregated over height and time, shown at 1-hour intervals starting from t = 1 h. The PDF maxima are marked by blue dots, with increasing color intensity representing later times. Right (orange axis): RMSE-based cost functions for parameter p (light orange curves) aggregated over height and time, shown at hourly intervals starting from t = 1 h. The cost function minima are marked by orange dots, with darker shading indicating later times. The default parameter value p = 2 is shown as a grey dashed line for reference.

In future work, we will test parameter estimation with the EAKF to objectively identify optimal flow-dependent turbulence parameters.

Results obtained from general stochastic estimation theory provide the benchmark against which ensemble-based parameter estimates can be assessed. A direct comparison, however, is not entirely straightforward because ensemble methods solve the inverse problem through an analysis scheme (Evensen, 2006) that implicitly minimizes a cost function (Zhang et al., 2020), assuming Gaussian error distributions and other simplifications that depend on the specific filter and its configuration. To mimic this behavior, we compute the root-mean-square error (RMSE) between the observations and the ensemble and track the parameter value that minimizes it. This reformulates the inverse problem as an optimization problem (Tarantola, 2005), similar to the implicit optimization performed by the EAKF. Unlike the stochastic inverse formulation, which explicitly accounts for uncertainty in the observations through the observation PDF, the RMSE cost function treats the observations as exact and attributes all mismatches to model error.

To test whether this optimization-based approach is a reasonable proxy, we compare it to the estimates from general inverse theory in Figure 6. As a proof of concept, this comparison is shown for parameter p, using a single-parameter perturbation ensemble of 10 000 members (more than sufficient to sample a one-dimensional parameter space). Restricting the perturbations

https://doi.org/10.5194/egusphere-2026-5554
Preprint. Discussion started: 5 November 2026
© Author(s) 2026. CC BY 4.0 License.

to a single parameter reduces sampling noise in the RMSE cost function, allowing its minimum to be clearly identified. This allows the evolution of the optimal parameter to be tracked in two ways: via the maxima of the posterior marginal distributions (as in Sect. 4.1), or via the minima of the cost functions. As expected, RMSE generally increases with forecast lead time (Fig. 6). This comparison yields two main insights. First, both methods produce a similar decrease in the optimal value of p, indicating that cost function minimization provides a reasonable approximation to general inverse theory. However, the relatively broad cost functions suggest that the optima are less constrained. Second, unlike posterior distributions, cost functions do not directly provide uncertainty estimates without additional assumptions. While the EAKF does provide an uncertainty estimate via its ensemble spread, this estimate is subject to well-recognized shortcomings: inter alia, the reliance on Gaussian distributions for the prior and observation errors, undersampling of the true uncertainty due to a finite ensemble size, and imperfect representation of model error. The stochastic inversion approach used in this study addresses the first of these directly by testing whether a Gaussian approximation is adequate, and the second by providing a well-sampled estimate of the parameter correlation structure that reveals which parameters are robustly constrained and which are more susceptible to sampling noise in a smaller ensemble.

6 Conclusions

This study explores the use of general stochastic inverse theory (Tarantola and Valette, 1982; Mosegaard and Tarantola, 2002) to investigate the flow-dependent behavior of parameters in a PBL parameterization scheme. Using a 27 000 member SCM ensemble constrained by synthetic θ observations from an LES, we examine three global parameters governing entrainment and mixing in the YSU PBL scheme: p, b, and A_e, which control the eddy diffusivity profile, the magnitude of countergradient correction, and the entrainment rate, respectively. Our main conclusions are as follows.

- Optimal values of p, b, and A_e vary with the atmospheric flow regime (Sect. 3 and 4.1), rather than remaining fixed across time. We argue that treating these empirically derived parameters as flow-dependent, rather than universal constants, potentially allows the model to compensate for structural error and better capture the parameterized process (Sect. 5.1).

- Joint posterior distributions informed by observations reveal correlations among parameters that are relevant for the design of perturbed parameter ensembles (Sect. 4.2). Rather than perturbing each parameter independently, these distributions identify physically plausible parameter combinations (Sect. 5.2), reducing the number of model integrations performed on unrealistic parameter sets.

- While general stochastic inverse theory serves as the theoretically optimal reference solution, its computational cost makes it impractical for realistic NWP applications. The results in Sect. 5.3 support cost-function minimization as a practical bridge between general inverse theory and ensemble-based methods, providing confidence that future parameter estimation experiments using the EAKF can recover similar parameter estimates while remaining computationally feasible for high-dimensional problems.

https://doi.org/10.5194/egusphere-2026-5554
Preprint. Discussion started: 5 November 2026
© Author(s) 2026. CC BY 4.0 License.

Building on this foundation, future work will employ the EAKF to objectively constrain turbulence parameters under (temporally) varying idealized atmospheric scenarios. Serafin and Weissmann (2025) laid the groundwork for this approach, addressing PE in a simplified first-order turbulence scheme and examining technical aspects of the assimilation (e.g., how the weight given to observations and background influences parameter convergence). The aim is to make PBL parameterization schemes adaptive to flow conditions, improving both their accuracy and flexibility. Characterizing the flow dependence of parameter estimates will be a key focus of this future work. In idealized settings, general stochastic inverse theory remains computationally feasible and can therefore serve as a valuable reference for the ensemble-based parameter estimates. Such a reference will not be available once parameter estimation is extended to operational NWP settings, where multiple sources of model error can project onto parameter updates (Ruckstuhl and Janjić, 2020). Establishing this correspondence under idealized conditions is therefore an important step toward interpreting the physical consistency of ensemble-based parameter updates.

Appendix A: Inverse problem formulation

According to Tarantola and Valette (1982), the most general formulation of inverse problem theory is characterized by the following three elements: (1) a prior probability distribution $f(\mathbf{m})$ carrying information we have on the model parameters $\mathbf{m}$, (2) a joint probability $f(\mathbf{y}^b, \mathbf{m})$ providing a description of modeling uncertainties, where $\mathbf{y}^b$ represents the model-predicted data (model equivalents), and (3) uncertain observations $f(\mathbf{y}^o)$. If we assume that the prior information on the model parameters and the observations are independent, the joint prior satisfies $f(\mathbf{y}^o,\mathbf{m}) = f(\mathbf{y}^o)f(\mathbf{m})$. The information we have on the inverse problem is now combined into a posterior probability density:

$$f(\mathbf{y}^b, \mathbf{m}, \mathbf{y}^o) = \frac{1}{\gamma} \frac{f(\mathbf{y}^o, \mathbf{m}) f(\mathbf{y}^b, \mathbf{m})}{\mu(\mathbf{y}^o, \mathbf{m})}, \tag{A1}$$

where $\mu(\mathbf{y}^o, \mathbf{m})$ is the homogeneous PDF representing null information, and γ is a normalization constant ensuring the posterior integrates to unity:

$$\gamma = \int_{Y^b \times Y^o \times M} \frac{f(\mathbf{y}^o, \mathbf{m}) f(\mathbf{y}^b, \mathbf{m})}{\mu(\mathbf{y}^o, \mathbf{m})} \, d\mathbf{y}^b \, d\mathbf{y}^o \, d\mathbf{m}. \tag{A2}$$

The goal is to find the marginal PDF $f_m(\mathbf{m})$ of model parameters from the joint posterior PDF:

$$f_m(\mathbf{m}) = \int_{Y^b \times Y^o} f(\mathbf{y}^b, \mathbf{m}, \mathbf{y}^o) d\mathbf{y}^b \, d\mathbf{y}^o. \tag{A3}$$

Although $\mathbf{y}^b$ and $\mathbf{y}^o$ occupy the same data space, in which case $\mathbf{y}^b$ is usually dropped, we retain $\mathbf{y}^b$ as a distinct argument throughout, consistent with its appearance in $f(\mathbf{y}^b, \mathbf{m})$.

Code and data availability. The code, data, and model versions used to produce the results in this work are archived on Zenodo and are available at https://doi.org/10.5281/zenodo.23856884 (Fritz, 2026). The archive includes copies of the original model versions used: WRFlux

https://doi.org/10.5194/egusphere-2026-5554
Preprint. Discussion started: 5 November 2026
© Author(s) 2026. CC BY 4.0 License.

v1.7.0, WRF v4.4.2, and DART-WRF v2024.2.20. The large-eddy simulation (LES) was run with WRFlux v1.7.0, and the corresponding namelist file and input sounding are provided in the archive. The single-column model (SCM) simulations were run with a modified version of WRF v4.4.2; the corresponding adjustments to the source code, namelist file, input sounding, and surface forcing file are provided in the archive. The ensemble simulations further required a modified version of DART-WRF, used here only to run an ensemble of forecasts, and the modified files are also in the Zenodo archive. The model output and the Jupyter notebook with which Figs. 1-6 can be reproduced are also available in the archive.

Author contributions. M.F. and St.S. conceptualized the study. M.F. conducted the experiments and analysis, and all co-authors were involved in the interpretation of the results. M.F. prepared the manuscript with contributions from all co-authors.

Competing interests. The authors declare that they have no conflict of interest.

Acknowledgements. This research has received financial support from the Vienna International School for Earth and Space Sciences (VISESS).

This research was funded in part by the Austrian Science Fund (FWF), under grant https://doi.org/10.55776/P37259. For open access purposes, the authors have applied a CC-BY public copyright license to any author-accepted manuscript version arising from this submission.

Computational resources were provided by Austrian Scientific Computing (ASC) and by the Department of Meteorology and Geophysics at the University of Vienna.

https://doi.org/10.5194/egusphere-2026-5554
Preprint. Discussion started: 5 November 2026
© Author(s) 2026. CC BY 4.0 License.

References

Anderson, J. L.: An Ensemble Adjustment Kalman Filter for Data Assimilation, Monthly Weather Review, 129, 2884–2903, https://doi.org/10.1175/1520-0493(2001)129<2884:AEAKFF>2.0.CO;2, 2001.

Ayotte, K. W., Sullivan, P. P., Andr n, A., Doney, S. C., Holtslag, A. A. M., Large, W. G., McWilliams, J. C., Moeng, C.-H., Otte, M. J., Tribbia, J. J., and Wyngaard, J. C.: An evaluation of neutral and convective planetary boundary-layer parameterizations relative to large eddy simulations, Boundary-Layer Meteorology, 79, 131–175, https://doi.org/10.1007/BF00120078, 1996.

Backus, G. and Gilbert, F.: Uniqueness in the inversion of inaccurate gross Earth data, Philosophical Transactions of the Royal Society of London, Series A: Mathematical and Physical Sciences, 266, 123–192, https://doi.org/10.1098/rsta.1970.0005, _eprint: https://royalsocietypublishing.org/rsta/article-pdf/266/1173/123/268003/rsta.1970.0005.pdf, 1970.

Bennett, A. F.: Inverse Methods in Physical Oceanography, Cambridge Monographs on Mechanics, Cambridge University Press, 1992.

Berner, J., Achatz, U., Batté, L., Bengtsson, L., Cámara, A. D. L., Christensen, H. M., Colangeli, M., Coleman, D. R. B., Crommelin, D., Dolaptchiev, S. I., Franzke, C. L. E., Friederichs, P., Imkeller, P., Järvinen, H., Juricke, S., Kitsios, V., Lott, F., Lucarini, V., Mahajan, S., Palmer, T. N., Penland, C., Sakradzija, M., Von Storch, J.-S., Weisheimer, A., Weniger, M., Williams, P. D., and Yano, J.-I.: Stochastic Parameterization: Toward a New View of Weather and Climate Models, Bulletin of the American Meteorological Society, 98, 565–588, https://doi.org/10.1175/BAMS-D-15-00268.1, 2017.

Bolstad, W. M. and Curran, J. M.: Introduction to Bayesian statistics, John Wiley & Sons, https://doi.org/10.1002/9780470181188, 2007.

Brost, R. and Wyngaard, J.: A model study of the stably stratified planetary boundary layer, Journal of Atmospheric Sciences, 35, 1427–1440, https://doi.org/10.1175/1520-0469(1978)035<1427:AMSOTS>2.0.CO;2, 1978.

Charara, M., Barnes, C., and Tarantola, A.: Full waveform inversion of seismic data for a viscoelastic medium, vol. 92, pp. 68–81, ISBN 978-3-540-65916-7, https://doi.org/10.1007/BFb0010284, 2000.

Cleary, E., Garbuno-Inigo, A., Lan, S., Schneider, T., and Stuart, A. M.: Calibrate, emulate, sample, Journal of Computational Physics, 424, 109 716, https://doi.org/10.1016/j.jcp.2020.109716, 2021.

Crase, E., Wideman, C., Noble, M., and Tarantola, A.: Nonlinear elastic waveform inversion of land seismic reflection data, Journal of Geophysical Research: Solid Earth, 97, 4685–4703, https://doi.org/https://doi.org/10.1029/90JB00832, 1992.

de Roode, S. R., Jonker, H. J., Duynkerke, P. G., and Stevens, B.: Countergradient fluxes of conserved variables in the clear convective and stratocumulus-topped boundary layer: The role of the entrainment flux, Boundary-layer meteorology, 112, 179–196, https://doi.org/10.1023/B:BOUN.0000020167.25780.16, 2004.

Dunbar, O. R. A., Garbuno-Inigo, A., Schneider, T., and Stuart, A. M.: Calibration and Uncertainty Quantification of Convective Parameters in an Idealized GCM, Journal of Advances in Modeling Earth Systems, 13, https://doi.org/10.1029/2020MS002454, 2021.

Edeling, W., Cinnella, P., Dwight, R., and Bijl, H.: Bayesian estimates of parameter variability in the k–ϵ turbulence model, Journal of Computational Physics, 258, 73–94, https://doi.org/10.1016/j.jcp.2013.10.027, 2014.

Ertel, H.: Der vertikale Turbulenz-Wärmestrom in der Atmosphäre., vol. 59, 1942.

Evensen, G.: Data assimilation: The Ensemble Kalman Filter, Springer-Verlag Berlin Heidelberg, ISBN 9783642037108, https://doi.org/10.1007/978-3-540-38301-7, 2006.

Fritz, M.: Code and data for "Flow dependence of boundary-layer scheme parameters revealed by stochastic inversion", Zenodo [Computer software], https://doi.org/10.5281/zenodo.23856884, 2026.

https://doi.org/10.5194/egusphere-2026-5554
Preprint. Discussion started: 5 November 2026
© Author(s) 2026. CC BY 4.0 License.



Göbel, M., Serafin, S., and Rotach, M. W.: Numerically consistent budgets of potential temperature, momentum, and moisture in Cartesian coordinates: application to the WRF model, Geoscientific Model Development, 15, 669–681, https://doi.org/10.5194/gmd-15-669-2022, 2022.

Grund, D. and Schemm, S.: Bayesian Calibration of a Large-Eddy Resolving Model Towards Campaign Measurements With an Ensemble Kalman Smoother, Journal of Advances in Modeling Earth Systems, 18, https://doi.org/10.1029/2026MS005758, 2026.

Hacker, J. P. and Snyder, C.: Ensemble Kalman Filter Assimilation of Fixed Screen-Height Observations in a Parameterized PBL, Monthly Weather Review, 133, 3260–3275, https://doi.org/10.1175/MWR3022.1, 2005.

Hacker, J. P., Snyder, C., Ha, S.-Y., and Pocernich, M.: Linear and non-linear response to parameter variations in a mesoscale model, Tellus A: Dynamic Meteorology and Oceanography, 63, 429, https://doi.org/10.1111/j.1600-0870.2010.00505.x, 2011.

Holtslag, A. A. M. and Boville, B. A.: Local Versus Nonlocal Boundary-Layer Diffusion in a Global Climate Model, Journal of Climate, 6, 1825–1842, https://doi.org/10.1175/1520-0442(1993)006<1825:LVNBLD>2.0.CO;2, 1993.

Hong, S.-Y., Noh, Y., and Dudhia, J.: A New Vertical Diffusion Package with an Explicit Treatment of Entrainment Processes, Monthly Weather Review, 134, 2318–2341, https://doi.org/10.1175/MWR3199.1, 2006.

Howland, M. F., Dunbar, O. R. A., and Schneider, T.: Parameter Uncertainty Quantification in an Idealized GCM With a Seasonal Cycle, Journal of Advances in Modeling Earth Systems, 14, https://doi.org/10.1029/2021MS002735, 2022.

Hu, X.-M., Klein, P. M., and Xue, M.: Evaluation of the updated YSU planetary boundary layer scheme within WRF for wind resource and air quality assessments, Journal of Geophysical Research: Atmospheres, 118, 10–490, https://doi.org/10.1002/jgrd.50823, 2013.

Kim, K., Lim, K., Lee, J., Kim, K., Wang, H., Qian, Y., Yoon, J., Lee, Y., Choi, H., and Lee, G.: Uncertainty quantification and optimization of precipitating hydrometeor parameters for winter precipitation in a cloud microphysics scheme, Atmospheric Research, 330, https://doi.org/10.1016/j.atmosres.2025.108554, publisher Copyright: © 2025 The Authors, 2026.

Mosegaard, K.: Quest for consistency, symmetry, and simplicity — The legacy of Albert Tarantola, Geophysics, 76, W51–W61, https://doi.org/10.1190/geo2010-0328.1, 2011.

Mosegaard, K. and Tarantola, A.: 16 - Probabilistic Approach to Inverse Problems, in: International Handbook of Earthquake and Engineering Seismology, Part A, edited by Lee, W. H., Kanamori, H., Jennings, P. C., and Kisslinger, C., vol. 81 of *International Geophysics*, pp. 237–265, Academic Press, https://doi.org/10.1016/S0074-6142(02)80219-4, 2002.

Murphy, J. M., Sexton, D. M. H., Barnett, D. N., Jones, G. S., Webb, M. J., Collins, M., and Stainforth, D. A.: Quantification of modelling uncertainties in a large ensemble of climate change simulations, Nature, 430, 768–772, https://doi.org/10.1038/nature02771, 2004.

Noh, Y., Cheon, W. G., Hong, S. Y., and Raasch, S.: Improvement of the K-profile Model for the Planetary Boundary Layer based on Large Eddy Simulation Data, Boundary-Layer Meteorology, 107, 401–427, https://doi.org/10.1023/A:1022146015946, 2003.

Ollinaho, P., Laine, M., Solonen, A., Haario, H., and Järvinen, H.: NWP model forecast skill optimization via closure parameter variations, Quarterly Journal of the Royal Meteorological Society, 139, 1520–1532, https://doi.org/10.1002/qj.2044, 2013.

O'Brien, J. J.: A note on the vertical structure of the eddy exchange coefficient in the planetary boundary layer, J. atmos. Sci, 27, 1213–1215, https://doi.org/10.1175/1520-0469(1970)027%3C1213:ANOTVS%3E2.0.CO;2, 1970.

Pleim, J. E.: A Combined Local and Nonlocal Closure Model for the Atmospheric Boundary Layer. Part I: Model Description and Testing, Journal of Applied Meteorology and Climatology, 46, 1383 – 1395, https://doi.org/10.1175/JAM2539.1, 2007.

Posselt, D. J. and Vukicevic, T.: Robust Characterization of Model Physics Uncertainty for Simulations of Deep Moist Convection, Monthly Weather Review, 138, 1513 – 1535, https://doi.org/10.1175/2009MWR3094.1, 2010.

https://doi.org/10.5194/egusphere-2026-5554
Preprint. Discussion started: 5 November 2026
© Author(s) 2026. CC BY 4.0 License.

Reynolds, C. A., Ridout, J. A., and McLay, J. G.: Examination of parameter variations in the U. S. Navy Global Ensemble, Tellus A: Dynamic Meteorology and Oceanography, 63, 841, https://doi.org/10.1111/j.1600-0870.2011.00532.x, 2011.

Rios-Berrios, R., Vukicevic, T., and Tang, B.: Adopting Model Uncertainties for Tropical Cyclone Intensity Prediction, Monthly Weather Review, 142, 72 – 78, https://doi.org/10.1175/MWR-D-13-00186.1, 2014.

Ruckstuhl, Y. and Janjić, T.: Combined State-Parameter Estimation with the LETKF for Convective-Scale Weather Forecasting, Monthly Weather Review, 148, 1607–1628, https://doi.org/10.1175/MWR-D-19-0233.1, 2020.

Saltelli, A., Annoni, P., Azzini, I., Campolongo, F., Ratto, M., and Tarantola, S.: Variance based sensitivity analysis of model output. Design and estimator for the total sensitivity index, Computer Physics Communications, 181, 259–270, https://doi.org/10.1016/j.cpc.2009.09.018, 2010.

Serafin, S. and Weissmann, M.: Can ensemble-based parameter estimation aid parameterization design?, Quarterly Journal of the Royal Meteorological Society, p. e5031, https://doi.org/10.1002/qj.5031, 2025.

Shin, E. Y. and Howland, M. F.: Accelerated Bayesian Calibration and Uncertainty Quantification of RANS Turbulence Model Parameters for Stratified Atmospheric Boundary Layer Flows, Boundary-Layer Meteorology, 192, 3, https://doi.org/10.1007/s10546-025-00945-6, 2026.

Shutts, G.: A kinetic energy backscatter algorithm for use in ensemble prediction systems, Quarterly Journal of the Royal Meteorological Society, 131, 3079–3102, https://doi.org/10.1256/qj.04.106, 2005.

Skamarock, W. C., Klemp, J. B., Dudhia, J., Gill, D. O., Liu, Z., Berner, J., Wang, W., Powers, J. G., Duda, M. G., Barker, D. M., and Huang, X.-Y.: A description of the advanced research WRF model version 4, Tech. rep., UCAR/NCAR, https://doi.org/10.5065/1dfh-6p97, 2019.

Stensrud, D. J.: Parameterization schemes: keys to understanding numerical weather prediction models, Cambridge University Press, https://doi.org/10.1017/CBO9780511812590, 2007.

Storm, B., Dudhia, J., Basu, S., Swift, A., and Giammanco, I.: Evaluation of the weather research and forecasting model on forecasting low-level jets: Implications for wind energy, Wind Energy: An International Journal for Progress and Applications in Wind Power Conversion Technology, 12, 81–90, https://doi.org/10.1002/we.288, 2009.

Stull, R. B.: An introduction to boundary layer meteorology, vol. 13, Springer Science & Business Media, https://doi.org/10.1007/978-94-009-3027-8, 1988.

Tarantola, A.: Inversion of seismic reflection data in the acoustic approximation, Geophysics, 49, 1259–1266, https://doi.org/10.1190/1.1441754, 1984.

Tarantola, A.: Inverse problem theory and methods for model parameter estimation, SIAM, https://doi.org/10.1137/1.9780898717921, 2005.

Tarantola, A. and Valette, B.: Inverse problems = Quest for information, Journal of geophysics, 50, 159–170, https://journal.geophysicsjournal.com/JofG/article/view/28, 1982.

Tikhonov, A. N., Goncharsky, A. V., Stepanov, V. V., and Yagola, A. G.: Regularization methods, pp. 7–63, Springer Netherlands, Dordrecht, ISBN 978-94-015-8480-7, https://doi.org/10.1007/978-94-015-8480-7_2, 1995.

Troen, I. B. and Mahrt, L.: A simple model of the atmospheric boundary layer; sensitivity to surface evaporation, Boundary-Layer Meteorology, 37, 129–148, https://doi.org/10.1007/BF00122760, 1986.

van Leeuwen, P. J. and Evensen, G.: Data Assimilation and Inverse Methods in Terms of a Probabilistic Formulation, Monthly Weather Review, 124, 2898 – 2913, https://doi.org/10.1175/1520-0493(1996)124<2898:DAAIMI>2.0.CO;2, 1996.

Vukicevic, T. and Posselt, D.: Analysis of the Impact of Model Nonlinearities in Inverse Problem Solving, Journal of the Atmospheric Sciences, 65, 2803 – 2823, https://doi.org/10.1175/2008JAS2534.1, 2008.

https://doi.org/10.5194/egusphere-2026-5554
Preprint. Discussion started: 5 November 2026
© Author(s) 2026. CC BY 4.0 License.



Vukicevic, T., Posselt, D. J., and Stankovic, A.: Sensitivity of Modeled Microphysics to Stochastically Perturbed Parameters, Journal of Advances in Modeling Earth Systems, 14, https://doi.org/10.1029/2021MS002933, 2022.

Weisheimer, A., Corti, S., Palmer, T., and Vitart, F.: Addressing model error through atmospheric stochastic physical parametrizations: impact on the coupled ECMWF seasonal forecasting system, Philosophical Transactions of the Royal Society A: Mathematical, Physical and Engineering Sciences, 372, 20130 290, https://doi.org/10.1098/rsta.2013.0290, _eprint: https://royalsocietypublishing.org/rsta/article-pdf/doi/10.1098/rsta.2013.0290/400398/rsta.2013.0290.pdf, 2014.

Zhang, X.-L., Michelén-Ströfer, C., and Xiao, H.: Regularized ensemble Kalman methods for inverse problems, Journal of Computational Physics, 416, 109 517, https://doi.org/10.1016/j.jcp.2020.109517, 2020.

Zupanski, D. and Zupanski, M.: Model Error Estimation Employing an Ensemble Data Assimilation Approach, Monthly Weather Review, 134, 1337–1354, https://doi.org/10.1175/MWR3125.1, 2006.